Defining the microglia response during the time course of chronic neurodegeneration

JVI Accepted Manuscript Posted Online 30 December 2015
J. Virol. doi:10.1128/JVI.02613-15

Defining the microglia response during the time course of chronic neurodegeneration

Running title: Microglia in neurodegeneration

James E. Vincenti, Lita Murphy, Kathleen Grabert, Barry W. McColl, Enrico Cancellotti, Tom C. Freeman[±] and Jean C. Manson[±*]

The Roslin Institute and Royal (Dick) School of Veterinary Studies, University of Edinburgh, Easter Bush, Midlothian EH25 9RG, United Kingdom

[±] Joint senior authors

Corresponding author:

*Professor Jean Manson: jean.manson@roslin.ed.ac.uk

Conflict of Interests

None of the authors have any conflict of interest relating to this study

Authors Contributions

JV, EC, TF and JM designed the study, JV conducted the research, JV, TF and JM analysed the data, JV, TF and JM wrote the manuscript. BM, KR, LM provided tools and expertise and provided a valuable review of the manuscript.

36 pages, 9 figures, 1 supplementary table
Abstract 248 words, Text 5470

Abstract

Inflammation has been proposed as a major component of neurodegenerative diseases although the precise role it plays has yet to be defined. We have examined the role of key contributors to this inflammatory process, microglia, the major resident immune cell population of the brain, in a prion disease model of chronic neurodegeneration. Initially, we performed an extensive reanalysis of a large study of prion disease, where the transcriptome of mouse brains had been monitored throughout the time-course of disease. Our analysis has provided a detailed classification of the disease-associated genes based on cell type of origin and gene function. This revealed that the genes up-regulated during disease, regardless of the strain of mouse or prion protein, are expressed predominately by activated microglia. In order to study the microglia contribution more specifically we established a mouse model of prion disease in which the 79A murine prion strain was introduced by an intraperitoneal route into BALB/cJ$^{Fms\text{-}EGFP/-}$ mice, which express Enhanced Green Fluorescent Protein (EGFP) under control of the *c-fms* operon. Samples were taken at time points during disease progression and histological analysis of the brain and transcriptional analysis of isolated microglia was carried out. The analysis of isolated microglia revealed a disease specific, highly pro-inflammatory signature in addition to an up-regulation of genes associated with metabolism and respiratory stress. This study strongly supports the growing recognition of the importance of microglia within the prion disease process and identifies the nature of the response through gene expression analysis of isolated microglia.

Importance

Inflammation has been proposed as a major component of neurodegenerative diseases. We have examined the role of key contributors to this inflammatory process, microglia, the major resident immune cell population of the brain, in a murine prion disease model of chronic neurodegeneration. Our study demonstrates that genes up-regulated throughout the disease process, are expressed predominately by microglia. A disease specific highly pro-inflammatory signature was observed in addition to an up-regulation of genes associated with metabolism and respiratory stress. This study strongly supports the growing recognition of the important contribution of microglia to a chronic neurodegenerative disease process.

Key Words

Microglia, Neurodegeneration, Prion

Introduction

Over several decades the neuron has been subject to the majority of research into protein misfolding diseases, but it is now apparent that glial cells are important players in the neurodegenerative process. Many protein misfolding diseases including Alzheimer's disease, Parkinson's disease and prion diseases demonstrate activation of glial cells in the brain during the course of disease alongside accumulation of misfolded protein but the precise role of the glial cells in the disease process is not known (1-4). Transmission of prion agents

47 to mice provides an excellent model for studying the timing of events during a chronic
48 process of a neurodegeneration associated with a misfolded protein. The time of inoculation
49 defines the starting point for the disease process and highly reproducible characteristics of
50 mouse-adapted prions include accumulation of a misfolded host protein, gliosis, neuronal
51 loss, distribution of brain lesions and the end point of terminal disease. Activation of glial
52 cells, both astrocytes and microglia, has been extensively documented as an early event in
53 the pathogenesis of protein misfolding diseases, occurring well before the onset of clinical
54 disease (1, 5-7).
55
56 Microglia are the major resident immune cell in the brain and in steady-state are considered
57 a heterogeneous population with density differences across brain regions (8). They display
58 region dependant functional signatures, which are enhanced further by age (9). Under
59 normal conditions microglia adopt a 'resting' phenotype where they continually survey their
60 immediate environment with extended processes (10).
61
62 Following detection of a pathological insult or any disturbance to homeostasis, microglia
63 adapt their phenotype from 'resting' to 'activated' whereby they modify both morphology
64 and biological function (10-12). Activated microglia have diverse functional phenotypes
65 dependent on the nature of the stimuli that are not readily apparent from their
66 morphology, and include a much wider repertoire than the classically defined M1 and M2
67 phenotypes (13-16). It has also been proposed that microglia can readily switch from one
68 phenotype to another (17-19) and are sensitive to peripheral immune system
69 communication (20-22). It is also clear that a complicated interconnected network of CNS

cells contribute to the activated 'profile' adopted by microglia with signalling from both astrocytes and neurons having particular impact (23-26).

The change of microglia from a resting to an activated state is one of the first pathological features of prion disease long before there is any evidence of neurodegeneration. Activated microglia are widely distributed in the brain and are thought to express low levels of inflammatory cytokines but high levels of transforming growth factor beta 1 (TGFB1) and prostaglandin E2 (PGE2) (7, 27).

This study aims to investigate the role of microglia through detailed analysis of their morphology and gene expression during the course of prion disease thereby providing new insights into the pathophysiology of neurodegenerative disease. We have used a prion disease agent as a model of neurodegeneration and taken an unbiased whole genome expression analysis approach, which has allowed us to provide an insight into the molecular processes central to microglia during the neurodegeneration, and highlight how this may impact disease development. A strong myeloid association was attributed to disease associated genes identified in our reanalysis supporting the growing recognition of the importance of microglia within the disease process. To further clarify microglial contribution we isolated microglia from prion infected mice and analysed their gene expression profile.

Material and methods

Reanalysis of Hwang et al. (2009) Data

The Hwang dataset (28) was downloaded from http://prion.systemsbiology.net. Quality control of these data was performed by Fios Genomics Ltd. (Edinburgh, Scotland) using the ArrayQualityMetrics (29) and 32 microarrays were removed due to poor quality leaving 386, both infected and uninfected, for reanalysis. The removal of arrays did not affect the overall balance of the dataset with a mean average of 2.5 ± 0.08 SE arrays per time point. Data normalisation was performed using the Robust Multiarray Average (RMA) expression measure (30).

Initial inspection of the data showed that there were no age-related trends present in the control animal data and these were not included in further analyses. Data from prion infected animals were loaded into BioLayout *Express*^{3D} (31) and a Pearson correlation matrix calculated, comparing the expression data from each probeset on the array against all other probesets ($P^2/2$ pairwise calculations, where P is the number of probesets).

A threshold of $r \geq 0.75$ was used and the resultant correlation graph visualised. To identify groups of co-expressed genes, the graph was clustered using the graph-based Markov clustering (MCL) algorithm (32) with the inflation value set at 2.2. The expression profile of each cluster was inspected, and clusters of genes differentially expressed during disease were isolated and individual gene profiles examined. Those with an unconvincing profile, i.e. their expression was weak or unrelated to disease progression, were removed. This left a

dataset comprising 492 genes in which there was high degree of confidence that their expression was up-regulated during disease.

Determination of Cell Type of Origin and Function of Disease-associated Transcripts

Cell origin was determined with reference to existing datasets. A dataset was compiled from data derived from a number of published studies and included microglia, macrophage and osteoclast myeloid populations (33, 34); purified neuronal populations derived from the cortex (cholecystokinin^{+ve}, cholinergic, layer 5a, layer 5b, layer 6, prepronociceptin^{+ve}); the striatum (dopamine receptor subtype-1 medium spiny, dopamine receptor subtype-2 medium spiny) and the cerebellum (basket, Golgi, purkinje, stellate, unipolar brush) and astrocytes, Bergman glia and oligodendrocyte populations (35, 36). Finally, datasets derived from macrophage cultures cultured with lipopolysaccharide (LPS) bacterial endotoxin (37) were included to allow for the identification of those genes associated with activation of the innate immune system. Following normalisation of the data, the 492 genes demonstrating differential expression in response to prion disease were identified in the composite dataset through matching of gene symbols, and incorporated into an expression file. Within BioLayout *Express*^{3D} each gene could then be assessed for their expression in one or more of these cell types.

Gene ontology enrichment was determined by uploading the Affymetrix chip ID of the disease-associated genes to the online Ensembl Biomart data mining tool (ensembl.org/biomart) using the *Mus musculus* genes dataset (Ensembl Genes 66). Filters were applied restricting results to the Affymetrix 430 2.0 chip probe sets. To increase

accuracy for correct selection of function, filters for gene ontology evidence code, domain and name were applied, with experimental evidence codes preferred.

Animals and Treatment

Groups of male and female BALB/cJ$^{Fms\text{-}EGFP/-}$ mice, expressing enhanced green fluorescent protein (EGFP) under control of the *c-fms* operon (part of the *Csfr1* promoter) (38), were sex matched and housed under standard conditions in groups of three to five. Food and water access was *ad libitum*. All mouse experiments were reviewed and approved by the local ethical review committee and performed under license from the UK Home Office in accordance with the United Kingdom Animal (Scientific Procedures) Act 1988. Mice aged at 16 weeks old were challenged by an intraperitoneal (i.p.) route with 0.02 ml of 1% w/v (in physiological saline) 79A infected or normal brain material (NBr) for control. At time points 35, 100, 150 and 200 days post-inoculation (dpi) mice were sacrificed (9 per group for immunohistochemical analysis and 4 per group for microglial extraction). All remaining mice (12 and 8 per group respectively), were assessed for clinical signs of prion disease from 150 dpi, and incubation times were calculated according to previously described protocols (39). These mice were sacrificed during terminal disease, or earlier if welfare required. Tissue sections from these mice were assessed for spongiform degeneration following previously described procedures by a scientist blinded to experimental design (40).

Tissue Preparation and Immunohistochemical Analysis

Brains were removed at the selected time points. Those to be used for immunohistochemistry were perfusion fixed with saline followed by 4% paraformaldehyde

(PFA), pH 7.4. Brain tissue was embedded in paraffin and cut into sections (6 µm). Antigen retrieval was performed in an autoclave at 121°C for 15 min in dH_2O and then incubated in formic acid (98%) for 10 min at room temperature. Endogenous peroxidase was blocked with 1% H_2O_2 (Sigma-Aldrich) in methanol for 10 min. All sections were blocked with serum-free protein block (Dako) or normal goat serum prior to incubation with the primary antibody. Sections were immunostained with monoclonal antibody (MAb) 6H4 (Prionics) recognizing residues 143-151 of murine PrP (0.5 µg ml^{-1}) (41). Negative control slides were treated overnight with mouse immunoglobulin control (Invitrogen). Antibody binding was detected with Vector ABC kit (Vector laboratories) and visualized with 3,3,-diaminobenzidine chromogen. All sections were counterstained with haematoxylin.

Brains for microglia morphology assessment were removed and immersed in 4% PFA for 24 h, rinsed in Hank's balanced salt solution (HBSS) before incubating for a further 24 h in 20% sucrose solution at 4°C. Tissues were rinsed with HBSS and snap frozen in isopentane at -40°C. Brains for microglial extraction were immersed in cold HBSS prior to processing (see microglial isolation procedure).

Quantification of Microglia Morphology/ Phenotype

Frozen brain tissue was sectioned at 25 µm on a freezing block microtome and sequential sections 300 µm apart were taken for analysis. Quantification of microglia activation status was established on cellular aggregation and morphology observed in BALBcJ$^{Fms\text{-}EGFP/-}$ sections based on the average number of microglia per 0.05 mm^2. Images for cell quantification were captured as a 50 optical slice z-stack at x10 magnification (Zeiss Plan-Neofluar 10x/0.30

objective) and compiled into a composite image using ImageJ software 1.48a. Quantification of EGFP cell number was performed using particle analysis within ImageJ. Microglia radius was performed on x10 Z stack compiled (reporting Z stacks) images taken at x40 magnification (Zeiss Plan-Neofluar x40 / 1.30 objective) captured from three standard locations within four brain regions: the dentate gyrus, cerebellum, medulla and thalamus. There was a minimum of 3 mice per group and additional images were recorded on adjacent sections if the total number of EGFP expressing microglia was below 50. Euclidean distance mapping was utilised to quantify changes in morphology and was performed using the 'region of interest' function within ImageJ.

Microglial isolation procedure

Brains harvested for microglial extraction were placed in cold HBSS and diced before processing immediately. Brains were dissociated using a GentleMACS™ Dissociator (Miltenyi Biotec) and Neural Tissue Dissociation Kit P (Miltenyi Biotec). The final cell pellet was re-suspended in 16 ml 35% Isotonic Percoll, split between two 15 ml tubes and carefully overlaid with 5 ml ice cold 0.1% DEPC treated HBSS. The resulting Percoll gradient was centrifuged at 400 g for 45 min at 4°C. The pellets were then suspended and recombined into a final volume of 5 ml ice cold 0.1 % DEPC treated HBSS. Cells were pelleted at 400 g for 5 min at 4°C using no brake, re-suspended in 90 µl ice cold MACs buffer (Miltenyi Biotec), 10 µl CD11b (microglia) microbeads (Miltenyi Biotec) and incubated at 4°C for 15 min with gentle rotation. Following incubation with microbeads, the cell suspension was washed in 1 ml ice cold MACs buffer at 300 g for 5 min at 4°C then re-suspended in 500 µl

ice cold MACs buffer. Cells were passed through magnetised LS columns (Miltenyi Biotec) following the manufacturer's protocol.

Verification of Microglial Purity

A subset of isolated cells predicted to be microglia were stained with PE anti-mouse CD11b (Cambridge Bioscience) and APC anti-mouse CD45 (Cambridge Bioscience). Isotype controls were prepared using PE Rat IgG2b (Cambridge Bioscience) and APC Rat IgG2a (Cambridge Bioscience) and a subset of unstained cells served both as negative control and verification of correct BALB/cJ$^{Fms\text{-}EGFP/-}$ genotype. Cell viability was determined using SYTOX® Blue dead cell stain (Thermofischer Scientific). All cell samples were analysed on a BD FACS Aria IIIu 4-laser/11 detector cell sorter running BD FACSDiva™ software (BD Biosciences). Subsequent analysis of FACS data was also performed using Summit v4.3 software (Dako/Beckham Coulter).

Microarray Analysis of Isolated Microglia

Isolated microglia cells were treated with TRIzol® Reagent (Life Technologies) according to manufacturer's protocol. Total RNA quality was checked on an Agilent 2100 Bioanalyzer. RNA samples with RIN value of >7.0 were passed as suitable for analysis and two representative samples at each time-point for control and disease were taken forward for analysis. RNA processing was handled by Ark Genomics (The Roslin Institute & R(D)SVS). RNA was converted to amplified double-stranded cDNA containing biotin using the NuGen Ovation picoSL WTA labelling kit (NuGen). The cDNA samples were hybridised to Affymetrix

Mouse Gene 1.1 arrays on a GeneTitan instrument (Affymetrix). Data was quality controlled, RNA normalised and subjected to network analysis as described above.

Results

The neurodegenerative disease process is associated with an inflammatory response which is microglial in origin

Initially, we performed a reanalysis of the data produced by Hwang *et al.* (2009): a transcriptomics analysis of brains of multiple strains of mice infected with different prion strains sampled at various stages of disease progression. These analyses were performed with a view to identifying genes associated with neurodegenerative disease progression. The Hwang data from diseased animals were analysed within BioLayout *Express*^{3D}. A correlation graph was generated using a Pearson threshold of $r \geq 0.75$, consisting of 21,550 nodes with 1,253,332 edges (Figure 1A). Clustering with MCL yielded 416 clusters. Each cluster represented genes that share a high degree of co-expression. The expression profile of the majority of the clusters revealed they had an expression profile that was not linked to the disease process. Two major clusters of genes did however exhibit an expression profile that increased with disease progression in all animal/prion strain combinations (Figure 1B). The largest of these clusters comprised 377 genes and a second contained 115 genes that were notable for their increased activation in C57/Bl6 models (Figure 1B). Following manual inspection of all individual profiles, a total of 492 genes associated with prion disease development were identified (Supplementary Table 1). All genes in each cluster followed a similar expression profile with an increase in expression starting at approximately half way through the incubation period.

Once disease association was determined, we next attempted to identify the cellular origin for each of the 492 differentially expressed genes in question. This was done by examining the expression of the disease-associated genes in the context of a panel of isolated cell populations. Datasets were sourced from the GNFv3 cell atlas (33, 34), RNA TRAP (35, 36) and serial macrophage cultures subjected to LPS (37). This revealed that 315 out of the 492 differentially expressed genes were solely or at least predominately expressed by myeloid populations, thereby indicating the majority were likely expressed by microglia within the brain. In contrast, 147 of the genes were expressed by multiple cell types, whilst only 30 were found to be specific to astrocytes, oligodendrocytes and neurons collectively (Figure 2). The original study by Hwang et al., (2009) identified 333 differentially expressed genes. By overlaying these 333 genes onto our chosen external datasets within BioLayout *Express*^{3D} it was found that 158 of the 333 genes were attributed to a myeloid origin. A further 18 were attributed to non-myeloid cell types. The remaining genes were classed as generic, implying the origin could be any cell within the brain and as such do not rule out a microglial component.

Histological Analysis of Microglial Activation and PrP Deposition

Following the identification of the predominantly myeloid origin of the prion disease signature, we chose next to confirm this observation by performing an analysis of microglia isolated from diseased brains. Our aim was to verify these findings and to obtain a more detailed analysis of the activation of microglia during disease. To do this we chose a mouse

269 passaged prion agent 79A, inoculated into BALB/cJ $^{Fms\text{-}EGFP/-}$ mice by an intraperitoneal route
270 with 0.02 ml of 1% w/v 79A brain homogenate as our model.
271
272 Clinical disease onset occurred 198.5 +/- 1.0 (SEM) dpi with signs including lethargy, hair
273 unkempt/loss and hunching all reported. Terminal disease occurred 229 +/- 3.6 dpi.
274 Pathological analysis of the vacuolation in the brain of terminal animals (n=6) confirmed
275 clinical disease and indicated that vacuolation was widespread by terminal stage of disease
276 presenting as typical for the 79A prion strain (42, 43).
277
278 PrP deposition assessed by immunohistochemistry using the 6H4 antibody was first
279 detected in the infected mice at 150 dpi and restricted to the medulla (Figure 3A/B). PrP
280 assessment at the terminal stage of disease identified heavy accumulation of fine punctate
281 particles throughout the majority of the brain, strongest in the thalamus and extending into
282 the medulla. To a lesser extent, deposition was also observed within the hippocampus, but
283 it was only occasionally found within the cortex. This is the deposition pattern typically
284 associated with 79A disease progression (42, 44). Microglial activation was observed in the
285 same areas as PrP deposition at 150 dpi (Figure 3C/D). Microglia in the NBr inoculated
286 controls demonstrated ramified appearance and greater microglia separation at ~50 µm
287 (Figure 3E/F).
288
289 Microglia were identified during the course of disease using EGFP expression and a
290 quantitative analysis performed on their density and radius, as a measurement of
291 morphological changes typically associated with the activation of microglia. Comparison to
292 animals that had been inoculated with uninfected NBr homogenate, we observed at 150 dpi

293 an approximate 50% (p = 0.029) increase of microglial cell number per 0.05 mm^2, within the
294 medulla of 79A infected mice (Figure 4A). Similarly, at 200 dpi an increase of microglia of
295 approximately 50% (p = 0.02) was observed within the thalamus. The intercellular distance
296 of microglial in control and unaffected regions was approximately 70-100 µm, while within
297 affected regions this was reduced to approximately 25 µm (Figure 4B). Cellular microglial
298 activation was also defined by a marked increase in the diameter of the central body while
299 there is a reduction in the length and number of processes projecting from it (45). An
300 average length of approximately 30 µm was observed for thalamic microglia at 100 days,
301 while at 200 dpi this is reduced to an average of 20 µm, indicating morphology associated
302 with activation. The reduction in radius is matched with an increase in Euclidean distance
303 by 1 µm, similar to that seen in the microglia in the thalamus, and indicative of shorter
304 thicker processes and a larger central body (Figure 4C-E). Thus the pathological analysis
305 confirmed that microglial activation and PrP disease associated protein deposition occurs by
306 150 dpi in restricted regions of the brain, and during the course of disease both extend into
307 multiple brain regions. There was no evidence of either PrP deposition or microglial
308 activation at 100 days in this model.
309
310 ***Microglial activation profile***

311 Microglia were isolated at day 35, 100, 150 and 200 dpi from 79A inoculated and control
312 animals. Isolated cells were stained with CD11b and CD45 fluorochrome conjugated
313 antibodies and sorted by FACS to confirm purity (Figure 5A-D). Adult microglia are typically
314 shown as $CD11b^{High}$ and $CD45^{Low}$ (46) and the lower than expected CD11b forward and side
315 scatter may be attributed to competition for available antigen between the CD11b

316 microbeads and CD11b-PE marker. The number of CD45^{high} cells, indicative of impurities in
317 the cell isolation process by monocyte contamination, was negligible. Non-specific binding
318 or auto-fluorescence was not observed. Cell viability was confirmed as 97% ± 0.43 SE.
319 Microglia purity was further confirmed from the expression profile of twenty cell-specific
320 genes representing the main cell groups found within the brain (Figure 5E). The presence of
321 CD11b^{positive} circulating or inflammatory monocytes was confirmed to be absent as
322 evidenced by the negligible expression of *Ly6c* or *Ccr2* (Supplementary Figure 1).
323
324 The process of isolation did not appear to adversely affect the microglia disease signature.
325 There was a clear difference between expression profiles of microglia isolated from diseased
326 mice and those collected from uninfected controls. Of note was the lack of increased
327 expression of metabolism genes that may be expected if cells were unduly stressed during
328 the isolation process. Staining with SYTOX® Blue also confirmed cells from both infected and
329 control animals were viable prior to RNA isolation. Additionally, on a bright field microscope,
330 isolated microglia presented with a rounded refractive appearance, indicative of healthy
331 viable cells.
332
333 RNA was extracted and microarray analysis was performed. Following this, the patterns of
334 gene expression were analysed within BioLayout *Express*^{3D}. The expression profile of each
335 cluster was individually checked to ensure familiarity with the dataset, and those with a
336 disease associated signature selected. This resulted in 741 genes that demonstrated an
337 increase in expression predominately at 200 dpi. The 741 genes were also organised into 2
338 large clusters which shared a very similar gene expression profile with a clear increase in
339 expression profile (shown averaged in Figure 6A). Animals inoculated with NBr material

showed no significant change in expression throughout the corresponding period. Using the 741 genes of interest, a sample-to-sample (array) level graph within BioLayout *Express*^{3D} was generated and confirmed the arrays from the 200 dpi time point had less correlation with the rest of the samples (Figure 6B).

Gene Enrichment Analysis

Enrichment analysis of the disease-associated microglial genes using the FuncAssociate 2.0 database (47), confirmed the enrichment ($p<0.001$) of the following functional gene descriptions; translation, energy production, immune response, interferon response and cell stress (Figure 7A). Immunological response comprised the single largest category in respect to total gene number. The signature included transcripts associated with proteolysis, NFkB-mediated cytokine cascades and innate immunity. The GO enrichment functional groups of mitochondria, ribosome, cell stress, apoptotic process and proliferation confirmed the presence of a significant metabolic signature associated with these genes.

Gene ontology was performed for each gene using the data made available on the Ensembl Biomart database to allow for functional associations to be determined (Figure 7B). Just under two thirds of the 741 identified differentially expressed genes were attributed to metabolism and the maintenance of homeostasis. The correct determination of differentially expressed metabolic genes to a specific cell type is only possible through the type of isolated cell type analysis presented here. Metabolic genes are typically expressed by all tissue cells types, making identification of the cellular origin from a mixed cell population impossible. Genes that were related to the immune response comprised just

363 under a quarter of the total. The 6% of genes associated with cytoskeletal changes and
364 migration were classed into their own groups respectively and included genes associated
365 with membrane reshuffling. This was to be expected as microglia are known to be highly
366 motile in the healthy brain environment (10). The increased expression of cytokines *Il1*, *Tnfa*
367 and *Csf1*, but not *Il6* or *Il10*, would suggest the response by microglia is lacking in the full
368 spectrum of cytokines expected from a classical form of activation via the myeloid
369 differentiation primary response 88 (MYD88)-dependant pathway (48). Pathway analysis of
370 this dataset within the Reactome database (49), revealed many of the elements of the
371 MYD88-independent pathway were represented by the differentially expressed genes
372 within this study. This is supported by the lack of differential expression of *Myd88* (Figure
373 7C). In addition, *Tgfb1* was not found to be differentially expressed by microglia during the
374 disease process (Figure 7D). Transcripts associated with Tgfb1 signalling, including Smad
375 anchor for receptor activation (*Zfyve9*), suppressor-of-cytokine-signalling 3, 4 and 5 (*Socs3-*
376 *5*) and ubiquitin specific peptidase 15 (*Usp15*) were also absent.
377
378 Determination of the sub-cellular component for each gene considered to be associated
379 with metabolism/homeostasis was performed from data obtained from the Ensembl
380 Biomart database. This enabled the location of many genes to be plotted onto a cellular
381 map and further organised by function (Figure 8). The identified cellular components
382 included a significant increase in expression of genes associated with ribosomes within the
383 rough endoplasmic reticulum and cytoplasm. Indeed, the bulk of the metabolic genes were
384 associated with the ribosomes, thereby implying an increase in ribosome numbers and/or
385 ribosome turnover, or an increase in protein synthesis. Also present was a significant

Journal of Virology

386 concentration of genes associated with proteolysis, including proteasome based
387 ubiquitination.
388
389 Consistent with the increase in metabolic load were a considerable number of genes
390 associated with oxidative phosphorylation and energy production in mitochondria, including
391 subunits for cytochrome-c oxidase, NADH dehydrogenase and lactate dehydrogenases; the
392 latter associated with breakdown of increased levels of lactate in situations of respiratory
393 stress (50). Also observed were DNA repair processes including expression of poly(ADP-
394 ribosyl)ation-14 (*Parp14*); a potent transcriptional regulator and DNA damage-dependant
395 nuclear protein (51, 52).
396
397 The association of the identified genes of interest with a specific function outside
398 metabolism/homeostasis was plotted onto a cellular map using ontology data obtained
399 from the Ensembl Biomart database. This enabled the location of each gene to be
400 determined and further organised by function (Figure 9). The overall expression profile from
401 this set of genes is one of robust pro-inflammatory myeloid cell activation. The increased
402 expression of lysosomal-associated membrane protein, ATPase proton pumps and
403 numerous lysosomal enzymes including cathepsins, histocompatibility subunits and genes
404 involved in membrane restructuring, strongly support antigen presentation and are a
405 hallmark of classically activated innate immune cells. Increased expression of surface marker
406 transcripts *Cd48*, *Cd86*, *Ccl8*, *Cxcl9*, *Cxcl13*, and *Tlr2* was also observed and all are typically
407 associated with a pro-inflammatory classical activation phenotype (16, 53-55).
408

Journal of Virology

Discussion

The dataset generated by Hwang, et al. (28) is uniquely placed among transcriptome datasets as it is the first to be fully comprehensive in terms of prion-related disease models, encompassing as it does multiple prion strains and host backgrounds. Our reanalysis of these data using a correlation network-based approach in combination with a cell origin classification system has given a unique, unbiased and informative whole genome approach. This allows identification not only of a core set of genes involved, but also of cell types associated with the neurodegenerative disease process. We identified a further 299 disease-associated genes not reported in the original study by Hwang, et al. (28) (Table 1). The original analysis focused on defining pathways associated with disease progression, which speculated a prominent neuronal contribution to the disease signature. However our reanalysis identified a large proportion of those previously identified genes to be of a myeloid origin with a strong myeloid association being attributed to 315 out of the 492 disease associated genes. This supports the growing recognition of the importance of microglia within the disease process. To further clarify microglial contribution we isolated microglia from prion infected mice and analysed their gene expression profile.

Experimental differences between the current study and that of Hwang, et al. (28) including route of infection, single cell type analysis and RNA amplification, potentially limit the ability to directly compare the results of the two studies. Having said this 107 genes were seen to be upregulated during disease progression in both studies and were primarily associated with an innate immune response (Supplementary Figure 1). We adopted an intraperitoneal route of infection as a “more natural” route of infection rather than the more commonly

used intracranial route to ensure that microglial activation was the result of a response to initial infection entering the CNS environment. With an intracranial route of infection the microglial response may be complicated by the injection procedure resulting in what has been termed as 'pre-priming' of microglia (56-58). A peripheral route would also encapsulate any microglial response to systemic inflammation; observed in prion disease following a peripheral route of infection (59), but not following an intracerebral route (60). However both studies arrive at the same conclusion; prion disease is associated with a chronic inflammatory response with microglia being central to the disease process.

The increase in levels of *Il1b*, *Tnfa* and *Csf1* strongly portray the microglial activation profile as pro-inflammatory and not one of atypical down-regulation or resolution of inflammation (61). The presence of a significant increase in transcripts involved with proteasome activity and major-histocompatibility mediated antigen presentation, combined with expression of *Cxcr3* ligand genes, offers a microglia activation state more akin to classically activated macrophages. That said, the lack of expression of *Infγ*, *Il6* and *Il33* by microglia, all well-defined pro-inflammatory cytokines (62-64) suggests an atypical inflammatory response. Also of note, and crucial to the maintenance of a chronic response to inflammatory cytokines, was that expression of *Nfkb1* remained stable despite an increase in expression of NFKB1 inhibitors (*Nfκbia*, *Nfκbib* and *Nfκbie*) which have been shown to inhibit formation of NFKB1 at the transcription stages (65).

The inflammatory phenotype typically associated with prion disease has been shown to be remarkably anti-inflammatory and dominated by the anti-inflammatory growth factor Tgf-β1 following injection by an intracerebral (66) or hippocampal stereotactic route (7, 61).

Found in the healthy brain, Tgf-β1 is a constitutively expressed protein intricately involved in microglia homeostasis (67-70). The lack of differential expression of *Tgfb1* within this dataset, suggests a lack of active TGF-β1 mediated signalling as a significant contributor to the disease response by microglia. There was also lack of significant increase in expression of *Usp15*, *Zfyve9* or *Socs3-5,* indicating no increased translocation of SMAD2/3 proteins or MAPK signalling; core intracellular complexes of the TGF-β1 signalling pathway (67, 71-73). TGF-β1 is required for the correct function of the blood brain barrier, and is itself unable to pass (74, 75). This therefore suggests that the increased expression of Tgf-β1 noted in other studies, is either attributable to the intracerebral inoculation or expressed by another group of cells from within the CNS.

Microglia are known to intricately interact with neurons (76-78), and numerous genes associated with axon elongation, synapse regulation and neurotransmitter release were observed to increase in expression within the isolated microglia dataset. This partners the expression of many axon and synapse genes with microglia and adds them to the growing body of evidence for microglial involvement in neuron regulation (79-83). It has been proposed that microglia kill prion infected neurons in a manner dependent upon the presence and degree of fibrillarity of misfolded protein (84). This single cell dataset supports the generation of a neurotoxic response from microglia with increased expression of *Il1b, Tnfa* and caspase-4 (*Casp4*) indicating active processing within caspase-1 mediated inflammasomes (85-87). Other pro-inflammatory genes found within this dataset, and reported to be neurotoxic, include matrix metalloproteinase 12 (*Mmp12*) (88) and prostaglandin-endoperoxide synthase 2 (*Ptgs2*) (89). The latter is known to be expressed in

prion disease (90, 91) and is a target of non-steroidal anti-inflammatory drugs (NSAIDs) used in clinical trials to treat neurodegenerative diseases by inhibiting prostaglandin synthesis (92).

Within this analysis microglia were shown to express a disease signature markedly more pro-inflammatory than that currently portrayed in the literature for prion disease, and more akin to other protein-misfolding diseases, notably Alzheimer's disease, in which microglia are observed as expressing a repertoire of pro-inflammatory cytokines including *Tnfa*, *Il1b* and *Il6* (93-95). The increased expression of cytokines *Il1b*, *Tnfa* and *Csf1*, but not *Il6* in this dataset suggests an activation profile that is specific to prion disease and likely also unique to the in-vivo environment since co-cultures of microglia and neurons in the presence of $PrP^{106-126}$ induces a stereotypic response with CD14 mediated detection of damaged neurons and increased expression of Il6 (96). This matches the stereotypic neurotoxic response observed in co-cultures of neurons in the presence of LPS activated microglia (97).

Our study demonstrated that genes up-regulated throughout the disease process, are expressed predominately by microglia. A disease specific highly pro-inflammatory signature was observed in addition to an up-regulation of genes associated with metabolism and respiratory stress. This study strongly supports the growing recognition of the important contribution of microglia to a chronic neurodegenerative disease process. Protein misfolding diseases typically have a very long pre-clinical phase in which there is a steady and progressive increase in misfolded protein deposition, neuroinflammation and synaptopathy as the disease progresses. Thus an understanding of the contributors to this pre-clinical

503 phase provides opportunities for devising early intervention strategies to limit the pathology
504 before damage becomes irreversible

Funding Information

505 This study was funded by DTA studentship from the BBSRC. The funders had no role in
506 study design, data collection and interpretation

Acknowledgements

We would like to acknowledge the extensive support and expertise of Mrs Aileen Boyle, Mrs Gillian McGregor, Ms Dawn Drummond and Mrs Sandra Mack for pathology services, Mrs Rebecca Hogan for animal care, Mr Bob Fleming and Dr Deborah Brown for assistance with bioimaging and to Ms Lynesay McKay for assistance with Miltenyi Biotec equipment.

GEO accession number: GSE72039

507

508 ***References***

509 1. **Williams AE, van Dam AM, Man-A-Hing WKH, Berkenbosch F, Eikelenboom P, Fraser H.**
510 1994. Cytokines, prostaglandins and lipocortin-1 are present in the brains of scrapie-infected
511 mice. Brain Research **654:**200-206.
512 2. **Betmouni S, Perry VH, Gordon JL.** 1996. Evidence for an early inflammatory response in the
513 central nervous system of mice with scrapie. Neuroscience **74:**1-5.
514 3. **Ye X, Scallet AC, Kascsak RJ, Carp RI.** 1998. Astrocytosis and amyloid deposition in scrapie-
515 infected hamsters. Brain Res **809:**277-287.
516 4. **Jebelli J, Su W, Hopkins S, Pocock J, Garden GA.** 2015. Glia: guardians, gluttons, or guides
517 for the maintenance of neuronal connectivity? Annals of the New York Academy of
518 Sciences**:**n/a-n/a.
519 5. **Williams A, Lucassen PJ, Ritchie D, Bruce M.** 1997. PrP Deposition, Microglial Activation, and
520 Neuronal Apoptosis in Murine Scrapie. Experimental Neurology **144:**433-438.

6. **Baker CA, Lu ZY, Zaitsev I, Manuelidis L.** 1999. Microglial Activation Varies in Different Models of Creutzfeldt-Jakob Disease. J. Virol. **73:**5089-5097.
7. **Cunningham C, Boche D, Perry VH.** 2002. Transforming growth factor β1, the dominant cytokine in murine prion disease: influence on inflammatory cytokine synthesis and alteration of vascular extracellular matrix. Neuropathol Appl Neurobiol **28:**107-119.
8. **Lawson LJ, Perry VH, Dri P, Gordon S.** 1990. Heterogeneity in the distribution and morphology of microglia in the normal adult mouse brain. Neuroscience **39:**151-170.
9. **Hart AD, Wyttenbach A, Perry VH, Teeling JL.** 2012. Age related changes in microglial phenotype vary between CNS regions: grey versus white matter differences. Brain, behavior, and immunity **26:**754-765.
10. **Nimmerjahn A, Kirchhoff F, Helmchen F.** 2005. Resting Microglial Cells Are Highly Dynamic Surveillants of Brain Parenchyma in Vivo. Science **308:**1314-1318.
11. **Davalos D, Grutzendler J, Yang G, Kim JV, Zuo Y, Jung S, Littman DR, Dustin ML, Gan WB.** 2005. ATP mediates rapid microglial response to local brain injury in vivo. Nature neuroscience **8:**752-758.
12. **Kozai TD, Vazquez AL, Weaver CL, Kim SG, Cui XT.** 2012. In vivo two-photon microscopy reveals immediate microglial reaction to implantation of microelectrode through extension of processes. Journal of neural engineering **9:**066001.
13. **Perry VH, Nicoll JAR, Holmes C.** 2010. Microglia in neurodegenerative disease. Nature Reviews Neurology **6:**193-201.
14. **Mosser DM, Edwards JP.** 2008. Exploring the full spectrum of macrophage activation. Nat Rev Immunol **8:**958-969.
15. **Xue J, Schmidt SV, Sander J, Draffehn A, Krebs W, Quester I, De Nardo D, Gohel TD, Emde M, Schmidleithner L, Ganesan H, Nino-Castro A, Mallmann MR, Labzin L, Theis H, Kraut M, Beyer M, Latz E, Freeman TC, Ulas T, Schultze JL.** 2014. Transcriptome-based network analysis reveals a spectrum model of human macrophage activation. Immunity **40:**274-288.
16. **Martinez FO, Sica A, Mantovani A, Locati M.** 2008. Macrophage activation and polarization. Frontiers in bioscience : a journal and virtual library **13:**453-461.
17. **Palin K, Cunningham C, Forse P, Perry VH, Platt N.** 2008. Systemic inflammation switches the inflammatory cytokine profile in CNS Wallerian degeneration. Neurobiology of disease **30:**19-29.
18. **Murray CL, Skelly DT, Cunningham C.** 2011. Exacerbation of CNS inflammation and neurodegeneration by systemic LPS treatment is independent of circulating IL-1beta and IL-6. Journal of neuroinflammation **8:**50.
19. **Field R, Campion S, Warren C, Murray C, Cunningham C.** 2010. Systemic challenge with the TLR3 agonist poly I:C induces amplified IFNalpha/beta and IL-1beta responses in the diseased brain and exacerbates chronic neurodegeneration. Brain, behavior, and immunity **24:**996-1007.
20. **Thomson CA, McColl A, Cavanagh J, Graham GJ.** 2014. Peripheral inflammation is associated with remote global gene expression changes in the brain. Journal of neuroinflammation **11:**73.
21. **Lunnon K, Teeling JL, Tutt AL, Cragg MS, Glennie MJ, Perry VH.** 2011. Systemic inflammation modulates Fc receptor expression on microglia during chronic neurodegeneration. J Immunol **186:**7215-7224.
22. **Combrinck MI, Perry VH, Cunningham C.** 2002. Peripheral infection evokes exaggerated sickness behaviour in pre-clinical murine prion disease. Neuroscience **112:**7-11.
23. **Perry VH, Teeling J.** 2013. Microglia and macrophages of the central nervous system: the contribution of microglia priming and systemic inflammation to chronic neurodegeneration. Seminars in immunopathology.
24. **Saura J.** 2007. Microglial cells in astroglial cultures: a cautionary note. Journal of neuroinflammation **4:**26.

25. **Lee M, Schwab C, McGeer PL.** 2011. Astrocytes are GABAergic cells that modulate microglial activity. Glia **59:**152-165.
26. **Cardona AE, Pioro EP, Sasse ME, Kostenko V, Cardona SM, Dijkstra IM, Huang D, Kidd G, Dombrowski S, Dutta R, Lee JC, Cook DN, Jung S, Lira SA, Littman DR, Ransohoff RM.** 2006. Control of microglial neurotoxicity by the fractalkine receptor. Nature neuroscience **9:**917-924.
27. **Boche D, Cunningham C, Docagne F, Scott H, Perry VH.** 2006. TGF[beta]1 regulates the inflammatory response during chronic neurodegeneration. Neurobiology of disease **22:**638-650.
28. **Hwang D, Lee IY, Yoo H, Gehlenborg N, Cho J-H, Petritis B, Baxter D, Pitstick R, Young R, Spicer D, Price ND, Hohmann JG, DeArmond SJ, Carlson GA, Hood LE.** 2009. A systems approach to prion disease. Mol Syst Biol **5:**252.
29. **Kauffmann A, Gentleman R, Huber W.** 2009. arrayQualityMetrics--a bioconductor package for quality assessment of microarray data. Bioinformatics (Oxford, England) **25:**415-416.
30. **Irizarry RA, Hobbs B, Collin F, Beazer-Barclay YD, Antonellis KJ, Scherf U, Speed TP.** 2003. Exploration, normalization, and summaries of high density oligonucleotide array probe level data. Biostatistics (Oxford, England) **4:**249-264.
31. **Freeman TC, Goldovsky L, Brosch M, van Dongen S, Mazière P, Grocock RJ, Freilich S, Thornton J, Enright AJ.** 2007. Construction, visualisation, and clustering of transcription networks from microarray expression data. PLoS Computational Biology **3:**2032-2042.
32. **Dongen V.** 2000. Performance criteria for graph clustering and Markov cluster experiments. CWI (Centre for Mathematics and Computer Science)**:**INS-R0012.
33. **Wu C, Orozco C, Boyer J, Leglise M, Goodale J, Batalov S, Hodge CL, Haase J, Janes J, Huss JW, 3rd, Su AI.** 2009. BioGPS: an extensible and customizable portal for querying and organizing gene annotation resources. Genome Biol **10:**2009-2010.
34. **Su AI, Cooke MP, Ching KA, Hakak Y, Walker JR, Wiltshire T, Orth AP, Vega RG, Sapinoso LM, Moqrich A, Patapoutian A, Hampton GM, Schultz PG, Hogenesch JB.** 2002. Large-scale analysis of the human and mouse transcriptomes. Proc Natl Acad Sci U S A **99:**4465-4470.
35. **Doyle JP, Dougherty JD, Heiman M, Schmidt EF, Stevens TR, Ma G, Bupp S, Shrestha P, Shah RD, Doughty ML, Gong S, Greengard P, Heintz N.** 2008. Application of a translational profiling approach for the comparative analysis of CNS cell types. Cell **135:**749-762.
36. **Heiman M, Schaefer A, Gong S, Peterson JD, Day M, Ramsey KE, Suarez-Farinas M, Schwarz C, Stephan DA, Surmeier DJ, Greengard P, Heintz N.** 2008. A translational profiling approach for the molecular characterization of CNS cell types. Cell **135:**738-748.
37. **Lattin JE, Schroder K, Su AI, Walker JR, Zhang J, Wiltshire T, Saijo K, Glass CK, Hume DA, Kellie S, Sweet MJ.** 2008. Expression analysis of G Protein-Coupled Receptors in mouse macrophages. Immunome Res **4:**1745-7580.
38. **Sasmono RT, Oceandy D, Pollard JW, Tong W, Pavli P, Wainwright BJ, Ostrowski MC, Himes SR, Hume DA.** 2003. A macrophage colony-stimulating factor receptor-green fluorescent protein transgene is expressed throughout the mononuclear phagocyte system of the mouse. Blood **101:**1155-1163.
39. **Dickinson AG, Meikle VM, Fraser H.** 1968. Identification of a gene which controls the incubation period of some strains of scrapie agent in mice. J Comp Pathol **78:**293-299.
40. **Fraser H, Dickinson AG.** 1967. Distribution of experimentally induced scrapie lesions in the brain. NATURE **216:**1310-1311.
41. **Korth C, Stierli B, Streit P, Moser M, Schaller O, Fischer R, Schulz-Schaeffer W, Kretzschmar H, Raeber A, Braun U, Ehrensperger F, Hornemann S, Glockshuber R, Riek R, Billeter M, Wuthrich K, Oesch B.** 1997. Prion (PrPSc)-specific epitope defined by a monoclonal antibody. Nature **390:**74-77.
42. **Cancellotti E, Bradford BM, Tuzi NL, Hickey RD, Brown D, Brown KL, Barron RM, Kisielewski D, Piccardo P, Manson JC.** 2010. Glycosylation of PrP^{C} determines timing of neuroinvasion

and targeting in the brain following transmissible spongiform encephalopathy infection by a peripheral route. J Virol **84:**3464-3475.

43. **Giese A, Brown DR, Groschup MH, Feldmann C, Haist I, Kretzschmar HA.** 1998. Role of Microglia in Neuronal Cell Death in Prion Disease. Brain Pathology **8:**449-457.
44. **Bruce ME.** 1993. Scrapie strain variation and mutation. Br Med Bull **49:**822-838.
45. **McGeer PL, Kawamata T, Walker DG, Akiyama H, Tooyama I, McGeer EG.** 1993. Microglia in degenerative neurological disease. Glia **7:**84-92.
46. **Ginhoux F, Greter M, Leboeuf M, Nandi S, See P, Gokhan S, Mehler MF, Conway SJ, Ng LG, Stanley ER, Samokhvalov IM, Merad M.** 2010. Fate mapping analysis reveals that adult microglia derive from primitive macrophages. Science **330:**841-845.
47. **Berriz GF, King OD, Bryant B, Sander C, Roth FP.** 2003. Characterizing gene sets with FuncAssociate. Bioinformatics **19:**2502-2504.
48. **Akira S, Takeda K.** 2004. Toll-like receptor signalling. Nat Rev Immunol **4:**499-511.
49. **Croft D, Mundo AF, Haw R, Milacic M, Weiser J, Wu G, Caudy M, Garapati P, Gillespie M, Kamdar MR, Jassal B, Jupe S, Matthews L, May B, Palatnik S, Rothfels K, Shamovsky V, Song H, Williams M, Birney E, Hermjakob H, Stein L, D'Eustachio P.** 2014. The Reactome pathway knowledgebase. Nucleic Acids Res **42:**D472-477.
50. **Brooks GA, Dubouchaud H, Brown M, Sicurello JP, Butz CE.** 1999. Role of mitochondrial lactate dehydrogenase and lactate oxidation in the intracellular lactate shuttle. Proc Natl Acad Sci U S A **96:**1129-1134.
51. **Ame JC, Spenlehauer C, de Murcia G.** 2004. The PARP superfamily. BioEssays : news and reviews in molecular, cellular and developmental biology **26:**882-893.
52. **Mehrotra P, Riley JP, Patel R, Li F, Voss L, Goenka S.** 2011. PARP-14 functions as a transcriptional switch for Stat6-dependent gene activation. The Journal of biological chemistry **286:**1767-1776.
53. **Mantovani A, Sica A, Sozzani S, Allavena P, Vecchi A, Locati M.** 2004. The chemokine system in diverse forms of macrophage activation and polarization. Trends in immunology **25:**677-686.
54. **Samuel D, Kroner A.** 2011. Repertoire of microglial and macrophage responses after spinal cord injury. Nat Rev Neurosci **12:**388-399.
55. **Elishmereni M, Levi-Schaffer F.** 2011. CD48: A co-stimulatory receptor of immunity. The international journal of biochemistry & cell biology **43:**25-28.
56. **Dantzer R.** 2004. Cytokine-induced sickness behaviour: a neuroimmune response to activation of innate immunity. European Journal of Pharmacology **500:**399-411.
57. **Lemstra AW, Groen in't Woud JCM, Hoozemans JJM, van Haastert ES, Rozemuller AJM, Eikelenboom P, van Gool WA.** 2007. Microglia activation in sepsis: a case-control study. Journal of neuroinflammation **4:**4-4.
58. **Quan N, Banks WA.** 2007. Brain-immune communication pathways. Brain, behavior, and immunity **21:**727-735.
59. **Newsom DM, Liggitt HD, O'Rourke K, Zhuang D, Schneider DA, Harrington RD.** 2011. Cytokine antibody array analysis in brain and periphery of scrapie-infected Tg338 mice. Comparative immunology, microbiology and infectious diseases **34:**387-397.
60. **Cunningham C, Wilcockson DC, Boche D, Perry VH.** 2005. Comparison of Inflammatory and Acute-Phase Responses in the Brain and Peripheral Organs of the ME7 Model of Prion Disease. J Virol **79:**5174-5184.
61. **Walsh DTP, Betmouni SD, Perry VHD.** 2001. Absence of Detectable IL-1[beta] Production in Murine Prion Disease: A Model of Chronic Neurodegeneration. [Article]. Journal of neuropathology and experimental neurology **60:**173-182.
62. **Romano M, Sironi M, Toniatti C, Polentarutti N, Fruscella P, Ghezzi P, Faggioni R, Luini W, van Hinsbergh V, Sozzani S, Bussolino F, Poli V, Ciliberto G, Mantovani A.** 1997. Role of IL-6

and Its Soluble Receptor in Induction of Chemokines and Leukocyte Recruitment. Immunity **6:**315-325.

63. **Schmitz J, Owyang A, Oldham E, Song Y, Murphy E, McClanahan TK, Zurawski G, Moshrefi M, Qin J, Li X, Gorman DM, Bazan JF, Kastelein RA.** 2005. IL-33, an interleukin-1-like cytokine that signals via the IL-1 receptor-related protein ST2 and induces T helper type 2-associated cytokines. Immunity **23:**479-490.

64. **Kakkar R, Hei H, Dobner S, Lee RT.** 2012. Interleukin 33 as a mechanically responsive cytokine secreted by living cells. The Journal of biological chemistry **287:**6941-6948.

65. **Arenzana-Seisdedos F, Thompson J, Rodriguez MS, Bachelerie F, Thomas D, Hay RT.** 1995. Inducible nuclear expression of newly synthesized I kappa B alpha negatively regulates DNA-binding and transcriptional activities of NF-kappa B. Molecular and cellular biology **15:**2689-2696.

66. **Baker CA, Manuelidis L.** 2003. Unique inflammatory RNA profiles of microglia in Creutzfeldt–Jakob disease. Proc Natl Acad Sci U S A **100:**675-679.

67. **Abutbul S, Shapiro J, Szaingurten-Solodkin I, Levy N, Carmy Y, Baron R, Jung S, Monsonego A.** 2012. TGF-beta signaling through SMAD2/3 induces the quiescent microglial phenotype within the CNS environment. Glia **60:**1160-1171.

68. **Fadok VA, Bratton DL, Konowal A, Freed PW, Westcott JY, Henson PM.** 1998. Macrophages that have ingested apoptotic cells in vitro inhibit proinflammatory cytokine production through autocrine/paracrine mechanisms involving TGF-beta, PGE2, and PAF. The Journal of clinical investigation **101:**890-898.

69. **Lodge PA, Sriram S.** 1996. Regulation of microglial activation by TGF-beta, IL-10, and CSF-1. J Leukoc Biol **60:**502-508.

70. **Butovsky O, Jedrychowski MP, Moore CS, Cialic R, Lanser AJ, Gabriely G, Koeglsperger T, Dake B, Wu PM, Doykan CE, Fanek Z, Liu L, Chen Z, Rothstein JD, Ransohoff RM, Gygi SP, Antel JP, Weiner HL.** 2014. Identification of a unique TGF-beta-dependent molecular and functional signature in microglia. Nature neuroscience **17:**131-143.

71. **Heldin CH, Miyazono K, ten Dijke P.** 1997. TGF-beta signalling from cell membrane to nucleus through SMAD proteins. Nature **390:**465-471.

72. **Tsukazaki T, Chiang TA, Davison AF, Attisano L, Wrana JL.** 1998. SARA, a FYVE domain protein that recruits Smad2 to the TGFbeta receptor. Cell **95:**779-791.

73. **Inui M, Manfrin A, Mamidi A, Martello G, Morsut L, Soligo S, Enzo E, Moro S, Polo S, Dupont S, Cordenonsi M, Piccolo S.** 2011. USP15 is a deubiquitylating enzyme for receptor-activated SMADs. Nature cell biology **13:**1368-1375.

74. **Kastin AJ, Akerstrom V, Pan W.** 2003. Circulating TGF-beta1 does not cross the intact blood-brain barrier. Journal of molecular neuroscience : MN **21:**43-48.

75. **Dohgu S, Yamauchi A, Takata F, Naito M, Tsuruo T, Higuchi S, Sawada Y, Kataoka Y.** 2004. Transforming growth factor-beta1 upregulates the tight junction and P-glycoprotein of brain microvascular endothelial cells. Cellular and molecular neurobiology **24:**491-497.

76. **Siskova Z, Tremblay ME.** 2013. Microglia and synapse: interactions in health and neurodegeneration. Neural plasticity **2013:**425845.

77. **Tremblay M-È, Lowery RL, Majewska AK.** 2010. Microglial interactions with synapses are modulated by visual experience. PLoS Biology **8:**e1000527.

78. **Chen Z, Jalabi W, Hu W, Park HJ, Gale JT, Kidd GJ, Bernatowicz R, Gossman ZC, Chen JT, Dutta R, Trapp BD.** 2014. Microglial displacement of inhibitory synapses provides neuroprotection in the adult brain. Nature communications **5:**4486.

79. **Ji K, Akgul G, Wollmuth LP, Tsirka SE.** 2013. Microglia Actively Regulate the Number of Functional Synapses. PLoS One **8:**e56293.

80. **Miyamoto A, Wake H, Moorhouse AJ, Nabekura J.** 2013. Microglia and synapse interactions: fine tuning neural circuits and candidate molecules. Frontiers In Cellular Neuroscience **7:**1-6.

81. **Vukovic J, Colditz MJ, Blackmore DG, Ruitenberg MJ, Bartlett PF.** 2012. Microglia modulate hippocampal neural precursor activity in response to exercise and aging. The Journal of neuroscience : the official journal of the Society for Neuroscience **32:**6435-6443.
82. **Schafer DP, Lehrman EK, Stevens B.** 2013. The "quad-partite" synapse: Microglia-synapse interactions in the developing and mature CNS. Glia **61:**24-36.
83. **Sogn C, Puchades M, Gundersen V.** 2013. Rare contacts between synapses and microglial processes containing high levels of Iba1 and actin - a postembedding immunogold study in the healthy rat brain. European Journal of Neuroscience**:**2030-2040.
84. **Bate C, Reid S, Williams A.** 2001. Killing of prion-damaged neurones by microglia. Neuroreport **12:**2589-2594.
85. **Franchi L, Eigenbrod T, Munoz-Planillo R, Nunez G.** 2009. The inflammasome: a caspase-1-activation platform that regulates immune responses and disease pathogenesis. Nat Immunol **10:**241-247.
86. **Martinon F, Tschopp J.** 2007. Inflammatory caspases and inflammasomes: master switches of inflammation. Cell Death Differ **14:**10-22.
87. **Sollberger G, Strittmatter GE, Kistowska M, French LE, Beer HD.** 2012. Caspase-4 is required for activation of inflammasomes. J Immunol **188:**1992-2000.
88. **Bai Y, Zhu Z, Gao Z, Kong Y.** 2014. TLR2 signaling directs NO-dependent MMP-9 induction in mouse microglia. Neuroscience letters **571:**5-10.
89. **Minghetti l.** 2004. Cyclooxygenase-2 (COX-2) in Inflammatory and Degenerative Brain Diseases. Journal of neuropathology and experimental neurology **63:**901-910.
90. **Minghetti L, Pocchiari M.** 2007. Cyclooxygenase-2, prostaglandin E2, and microglial activation in prion diseases. International review of neurobiology **82:**265-275.
91. **Walsh DT, Perry VH, Minghetti L.** 2000. Cyclooxygenase-2 is highly expressed in microglial-like cells in a murine model of prion disease. Glia **29:**392-396.
92. **Vane JR.** 1971. Inhibition of prostaglandin synthesis as a mechanism of action for aspirin-like drugs. Nature: New biology **231:**232-235.
93. **Bhaskar K, Maphis N, Xu G, Varvel NH, Kokiko-Cochran ON, Weick JP, Staugaitis SM, Cardona A, Ransohoff RM, Herrup K, Lamb BT.** 2014. Microglial derived tumor necrosis factor-alpha drives Alzheimer's disease-related neuronal cell cycle events. Neurobiology of disease **62:**273-285.
94. **Griffin WS, Sheng JG, Roberts GW, Mrak RE.** 1995. Interleukin-1 expression in different plaque types in Alzheimer's disease: significance in plaque evolution. Journal of neuropathology and experimental neurology **54:**276-281.
95. **Tarkowski E, Blennow K, Wallin A, Tarkowski A.** 1999. Intracerebral production of tumor necrosis factor-alpha, a local neuroprotective agent, in Alzheimer disease and vascular dementia. Journal of clinical immunology **19:**223-230.
96. **Bate C, Boshuizen R, Williams A.** 2005. Microglial cells kill prion-damaged neurons in vitro by a CD14-dependent process. J Neuroimmunol **170:**62-70.
97. **Chao CC, Hu S, Molitor TW, Shaskan EG, Peterson PK.** 1992. Activated microglia mediate neuronal cell injury via a nitric oxide mechanism. J Immunol **149:**2736-2741.

Figure Legends

Figure 1* - BioLayout *Express*^{3D} *generated transcript -to-transcript network graph of selected genes of interest.

A: The list of 492 genes of interest with an expression pattern indicative of disease association were organised into 2 main clusters within BioLayout *Express*^{3D} by MCL. The green cluster comprising 410 nodes was joined by 29,339 edges indicating a high degree of co-expression between genes. The smaller purple cluster comprised 67 nodes and 1453 edges. **B:** The disease associated gene expression signatures of both clusters, displayed as a mean expression profile for each strain, revealed an up-regulation at approx. 50% of incubation period. The profile was similar for all genes in all mouse/prion combinations. The smaller purple cluster was expressed highest in BL6 strains resulting in the formation of a separate cluster. Error bars equate to ± SE. Grey triangles on X-axis indicate the incubation period between the point of inoculation to cull, some mouse/TSE strains leading to pathology and death faster than others.

Figure 2 - ***Cross reference of the 492 disease associated genes with co-normalised external datasets within* BioLayout *Express*^{3D}*.***

Within BioLayout E*xpress*^{3D} each gene of interest was classed and coloured as a specific cell type. Note how the previously determined MCL clusters are both dominated by myeloid derived genes (green). Genes associated with myeloid were divided into two groups based on sole association with myeloid cell types or in which sole origin could not be determined. Sole myeloid origin comprised 318 genes or 64% of the gene set. A total of 146 genes were associated with multiple cell types found within the CNS. Here a myeloid component was

still observed as strongly associated with the group. Genes assigned to astrocytes, oligodendrocytes and neurons were each represented by <20 genes.

Figure 3 - PrP Deposition and Microglia Activation Assessed by immunohistochemistry

Microglia activation was observed in the same areas as PrP deposition. **A/B:** Earliest accumulation of PrP (6H4) is at 150 dpi in the Medulla. Microglia can be seen **C/D:** as accumulating in the same areas of deposition. **E/F:** Normal Microglia in the thalamus and medulla respectively of mice challenged with normal brain demonstrate a ramified appearance and greater separation at ~ 50 µm. All images representative. Scale bars equate to 100 µm.

Figure 4 - Software determined quantification of EGFP expressing microglia in 79A infected BALB/cJ$^{Fms\text{-}EGFP/-}$ mice.

A: Quantification of regional microglia cell number in BALB/cJ$^{Fms\text{-}EGFP/-}$ mice following i.p. challenge with 79A at 100, 150 and 200 dpi. EGFP expressing cells were counting using ImageJ particle analysis function on x10 magnification 25µm Z-stack compiled images each comprising 50 optical slices. Microglia density increases in the medulla by ~ 50% at 150 dpi whereupon numbers remain constant in this region as PrP deposition spreads anteriorly. By 200 dpi microglia density in the thalamus has increased by ~ 100%. **B:** EGFP expressing microglia in the thalamus of BALB/cJ$^{Fms\text{-}EGFP/-}$ mice following i.p. challenge with 79A at 150 and 200 dpi. No difference in the number of EGFP expressing cells was observed in the

thalamus until 200 dpi when a concentration of reactive microglia spaced less than 25 µm was observed. Before 200 dpi microglia were observed in all animals as spaced at 50 - 100 µm and adopt a normal ramified morphology. Scale bars equate to 200 µm. Inset scale bars equate to 20 µm. **C:** At 200 dpi, microglia present with an engorged central body and shortened processes conferring a significant reduction in radius. D: Euclidean distance mapping affords a highly sensitive quantification of cell complexity encompassing both cell body size and process branching. The reduction in cell radius at 200 dpi is reflected in a mean Euclidean distance increase of 1 µm. Distance mapping also detailed a slightly less complex cell type in the NBr animals. **E:** High Resolution image analysis of microglia density per 0.05 mm^2 in the thalamus at 200 dpi revealed an increase of ~ 100%. † Comprises mean for all NBr inoculated BALB/cJ$^{Fms\text{-}EGFP/-}$ mice at all serial investigation time points. ǂ Mean statistical value determined using *t*-Test assuming variances determined by *f*-Test. *NS* = Not Significant. A, C-E: error bars equate to ± SE.

Figure 5 - Purity of isolated microglia was confirmed to be high and extracted RNA was confirmed to be of workable quality.

A: FACS sample analysis of CD11b microbead purified microglia stained with, and positive for, CD11b-PE & CD45-APC demonstrate a high purity. **B:** Isotope control and **C**: negative control show no non-specific binding or auto-fluorescence respectively. **D:** Cell viability was confirmed using SYTOX® live-dead stain. Inset: Isolated cells are EGFP positive. **E:** Plot of the mean expression profile of twenty genes known to be expressed in a cell-specific manner. The first five are known microglial expressed genes, the remainder are expressed in other brain cell types. This demonstrates that the expression of non-microglia genes in isolated

837 microglial populations is negligible, suggesting a relatively pure microglial population. Error
838 bars equate to ± SE.
839
840 ***Figure 6* - BioLayout *Express*^{3D} *analysis of isolated microglia gene expression.***

841 **A:** Average expression profile of the 2 large clusters produced within BioLayout *Express*^{3D} by
842 the 741 genes that demonstrate a differential expression in response to disease. All genes
843 yielded an increase in expression with a large escalation at 200 dpi in 79A infected mice.
844 Error bars equate to ± SE. **B:** Global microarray sample-to-sample transposed BioLayout
845 *Express*^{3D} graph of the 741 identified genes of interest. Prion infected and uninfected pre-
846 200 dpi arrays are highly correlated and organised into one component. Displaying high
847 inter-correlation but lower correlation with the rest of the population are the arrays for the
848 200 dpi infected group. Note: nodes have been coloured only for clarity and are not
849 indicative of MCL clustering.
850
851 ***Figure 7 - Ontological analysis of the microglia activation signature within the 741 genes***
852 ***of interest.***

853 **A:** GO enrichment terms determined from the identified 741 differentially expressed genes
854 using FuncAssociate 2.0 revealed protein translation, respiration, cellular stress and
855 components of the myeloid immune system to be significantly represented. All terms have
856 a *P*-value of considerably less than 0.001. **B:** Regulated disease-associated genes allocated
857 by function. Using the Ensembl Biomart database the majority of the regulated genes were
858 ascribed to metabolism and homeostasis. Genes associated with immune system, for which
859 differentiation has been included, comprise only a fifth. This highlights the power of a signal

cell isolation in correctly determining the association of metabolic genes with a specific cell type. **C**: Expression of inflammatory cytokines and transcription factors associated with the regulation of activation phenotype of microglia. Strong increase in expression of *Tnfa* and *Il1b,* but not cytokines associated with recruitment and escalation toward acquired immunity imply a disease-specific signature. **D:** Nominal and unchanged expression of *Tgfb1* is matched by a lack of expression of downstream transcripts mediated by TGFB1 activity. C-D error bars equate to ± SE.

Figure 8 - Genes of interest associated with metabolism and homeostasis.

A considerable number of genes with an increase in expression are associated with protein translation and processing. The increased metabolic load is reflected in the increase in expression of genes associated with energy production.

Figure 9 - Genes of interest associated with immune activation and cell-to-cell signalling.

Genes have been grouped by both function and cellular location. The signature is one of robust pro-inflammatory innate immune activation.

Figure 1

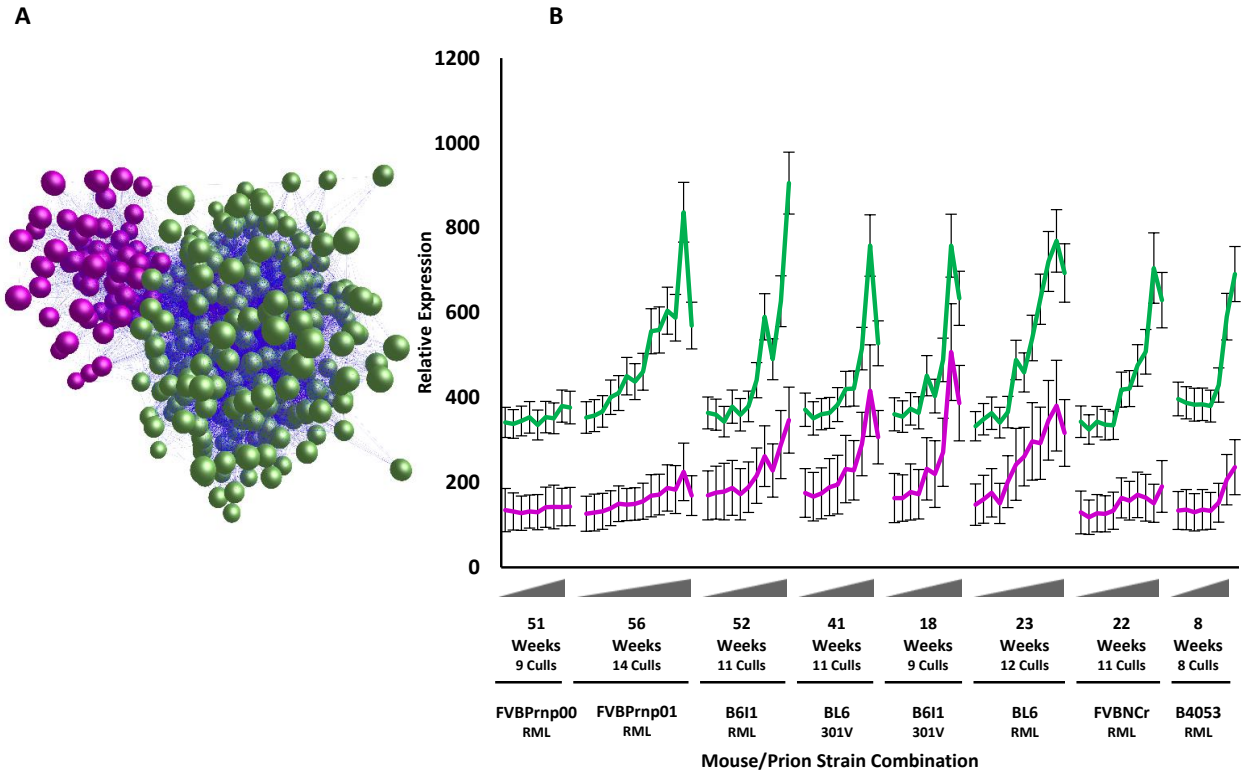

Figure 2

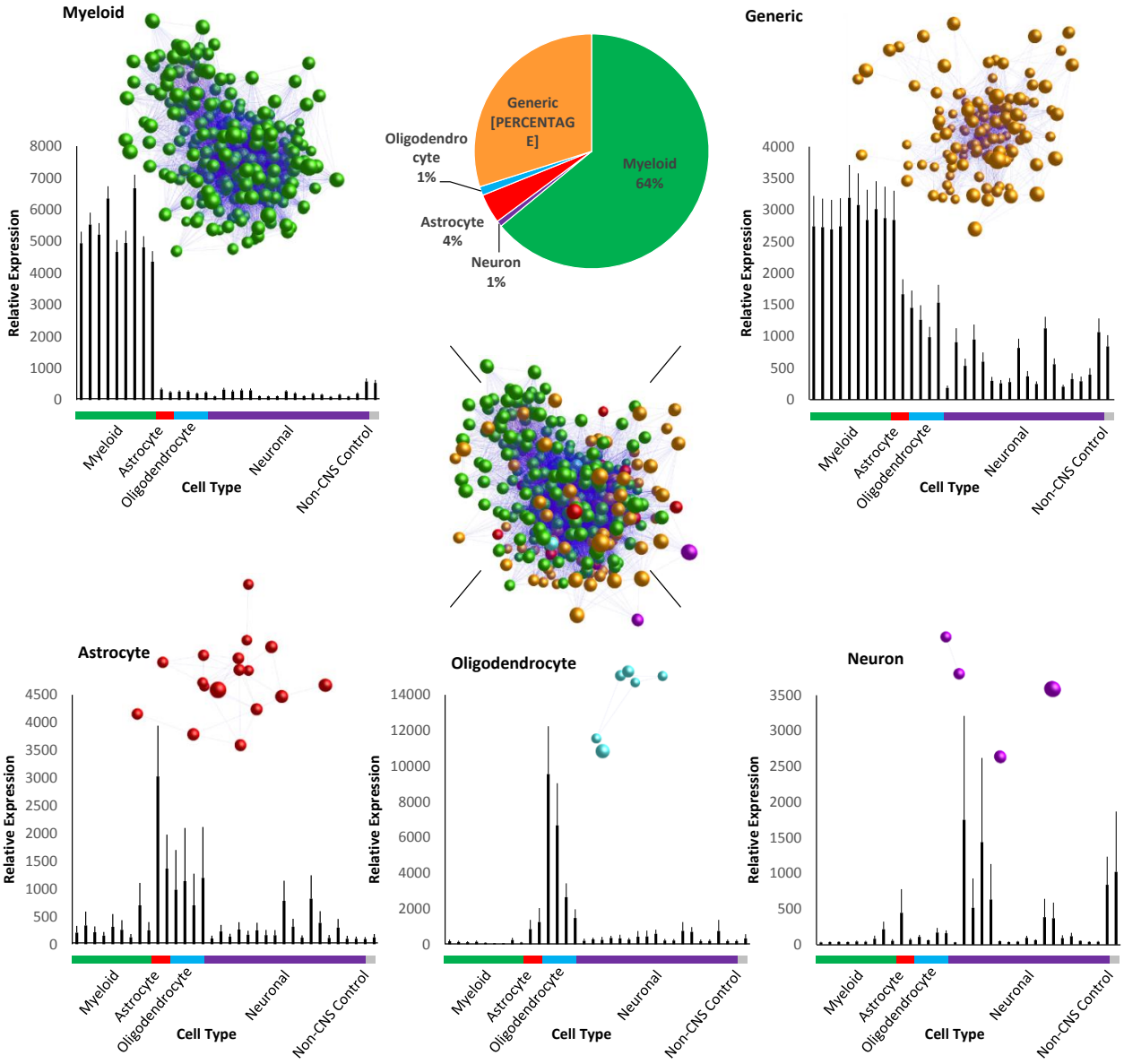

Figure 3

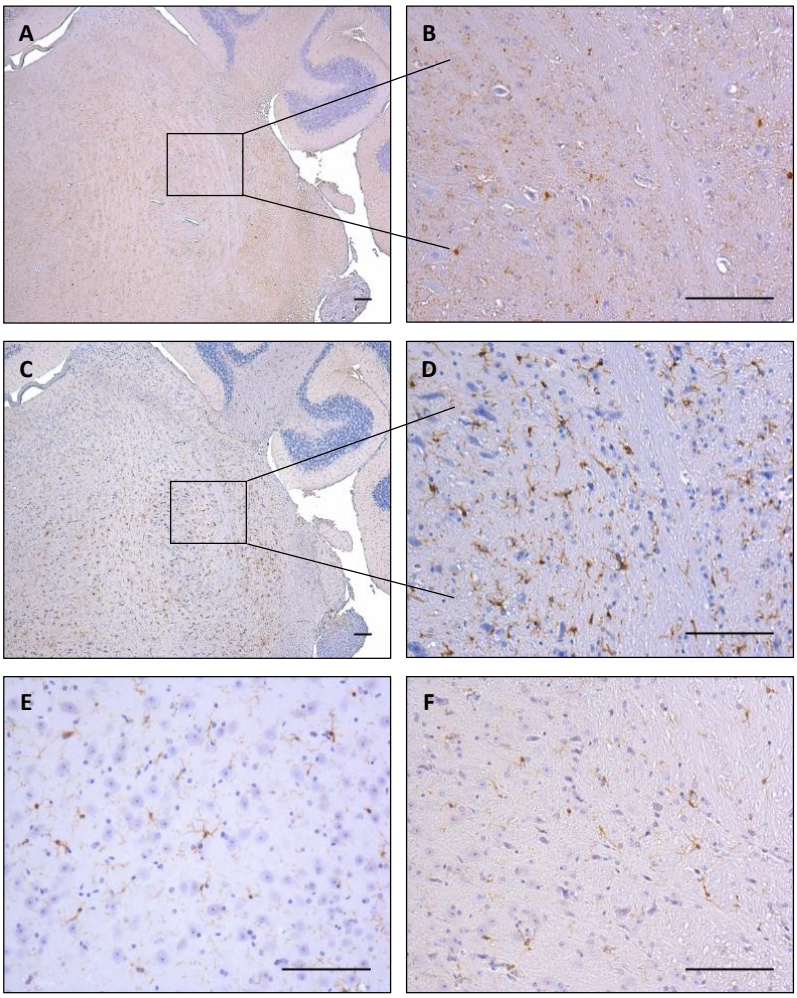

Figure 4

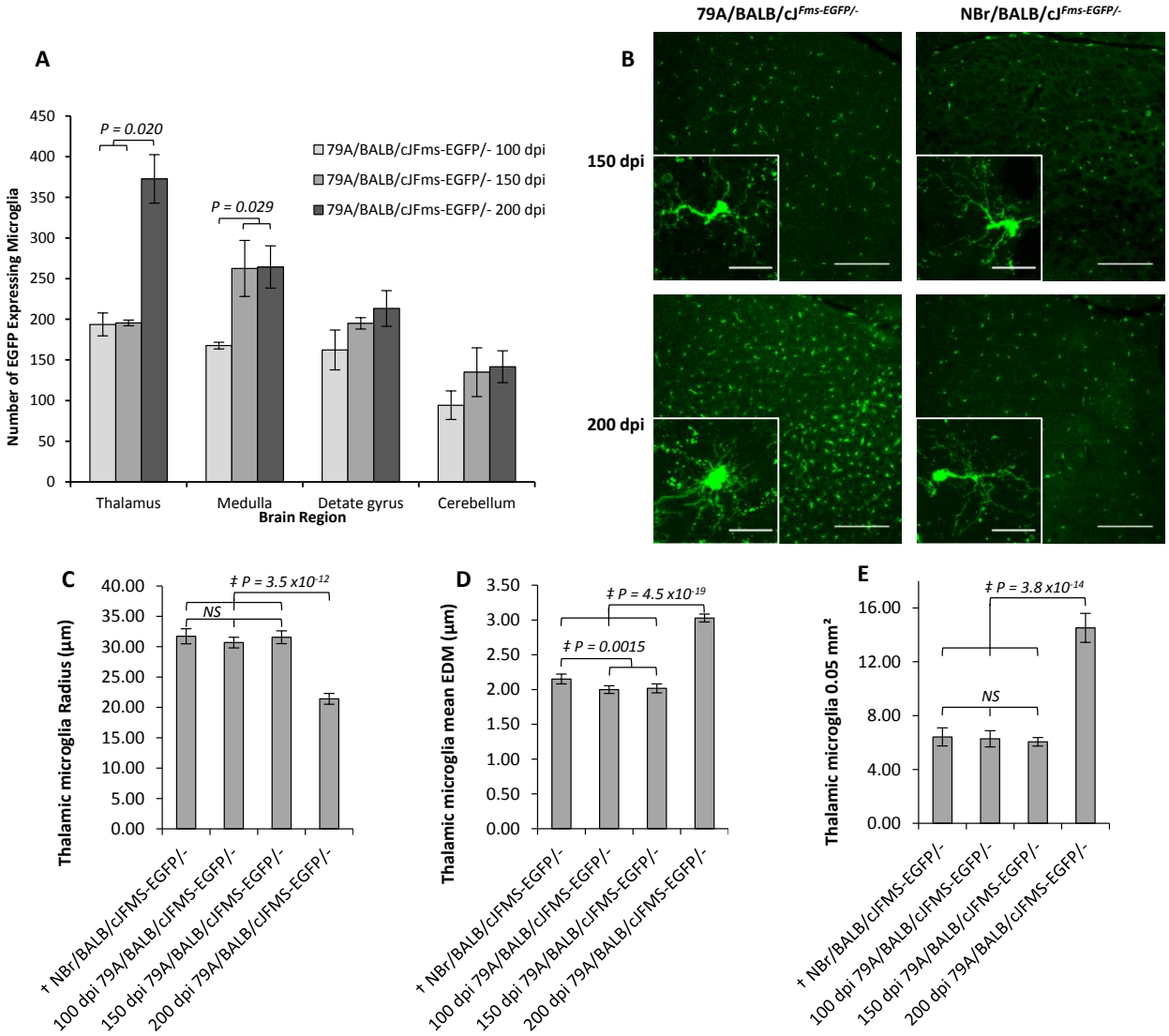

Figure 5

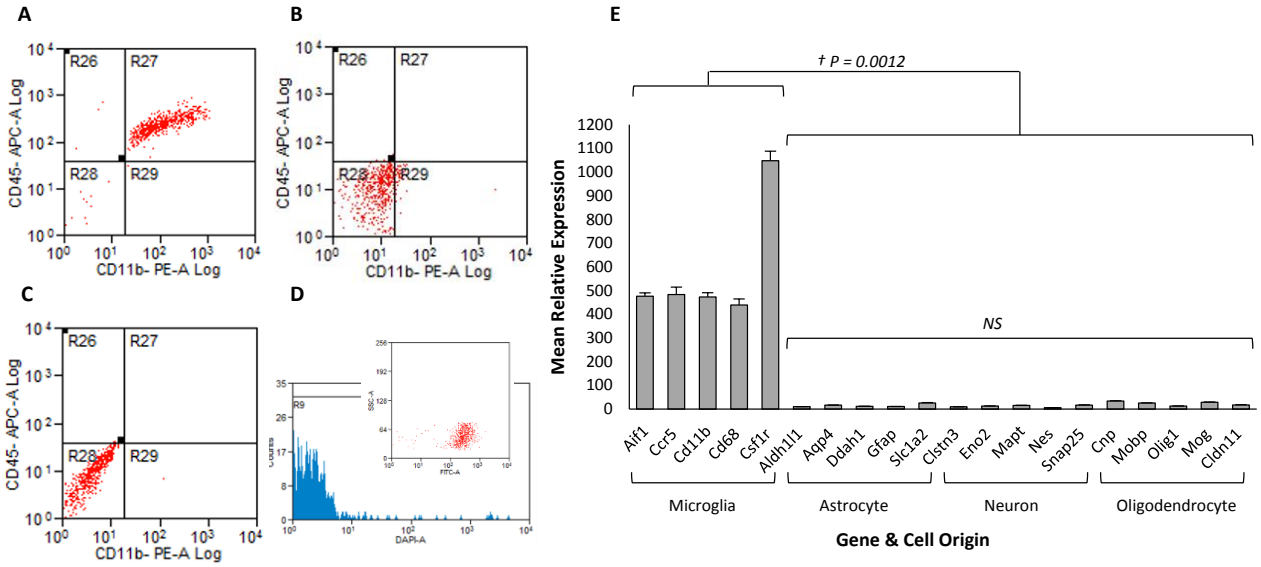

Figure 6

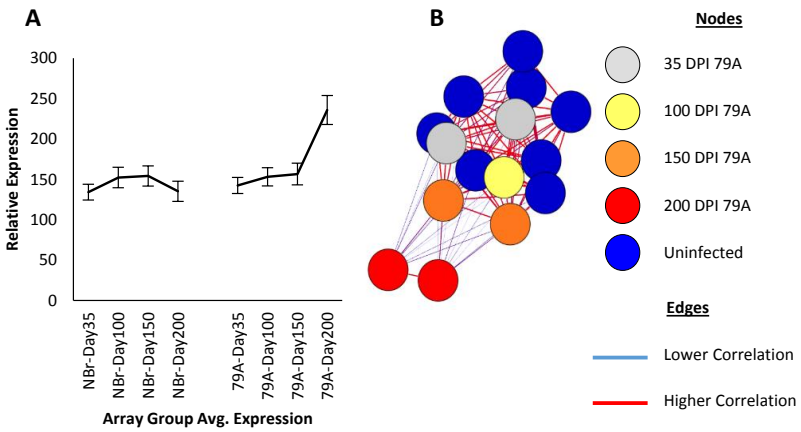

Figure 7

A

GO Ontological Annotation	GO ID	*P*-value	Gene No.	% Within Dataset
Protein Translation				
• ribosome	GO:0005840	6.37×10^{-54}	72	9.72
• translation	GO:0006412	3.52×10^{-26}	67	9.04
• ribosome biogenesis	GO:0042254	2.70×10^{-12}	27	3.64
• endoplasmic reticulum	GO:0005783	1.11×10^{-05}	68	9.18
Energy Production				
• mitochondrion	GO:0005739	1.10×10^{-13}	111	14.98
• generation of precursor metabolites and energy	GO:0006091	1.94×10^{-05}	21	2.83
• respiratory chain	GO:0070469	1.92×10^{-13}	19	2.56
Immune Response				
• lysosome	GO:0005764	1.55×10^{-12}	42	5.67
• regulation of cytokine production	GO:0001817	1.47×10^{-09}	38	5.13
• chemokine receptor binding	GO:0042379	2.20×10^{-09}	13	1.75
• regulation of locomotion	GO:0040012	1.03×10^{-07}	41	5.53
• endosome	GO:0005768	6.35×10^{-07}	41	5.53
• cell proliferation	GO:0008283	3.00×10^{-06}	78	10.53
• I-kappaB kinase/NF-kappaB cascade	GO:0007249	8.03×10^{-06}	19	2.56
• innate immune response-activating signal transduction	GO:0002758	1.38×10^{-05}	12	1.62
Interferon Response				
• response to interferon-gamma	GO:0034341	1.32×10^{-07}	12	1.62
• response to interferon-beta	GO:0035456	1.60×10^{-07}	9	1.21
• response to type I interferon	GO:0034340	8.99×10^{-07}	7	0.94
Cell Stress				
• response to stress	GO:0006950	2.53×10^{-13}	138	18.62
• apoptotic process	GO:0006915	5.05×10^{-07}	82	11.07
• response to wounding	GO:0009611	3.06×10^{-06}	45	6.07

B

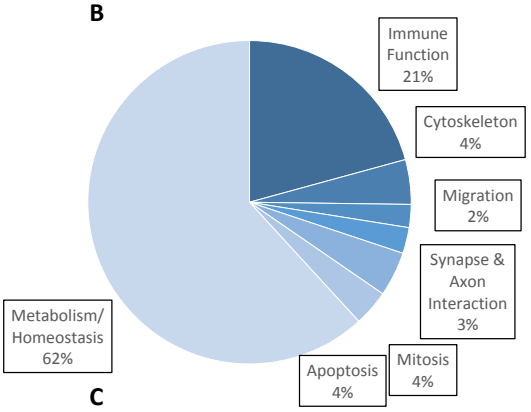

C

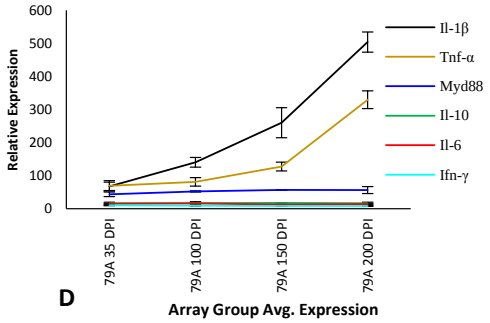

D

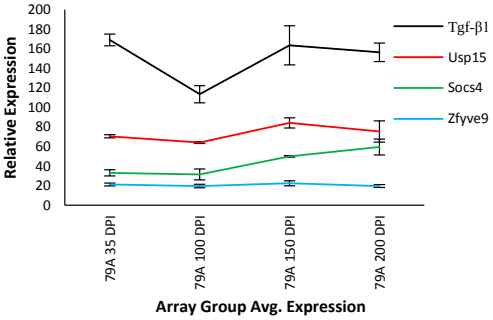

Figure 8

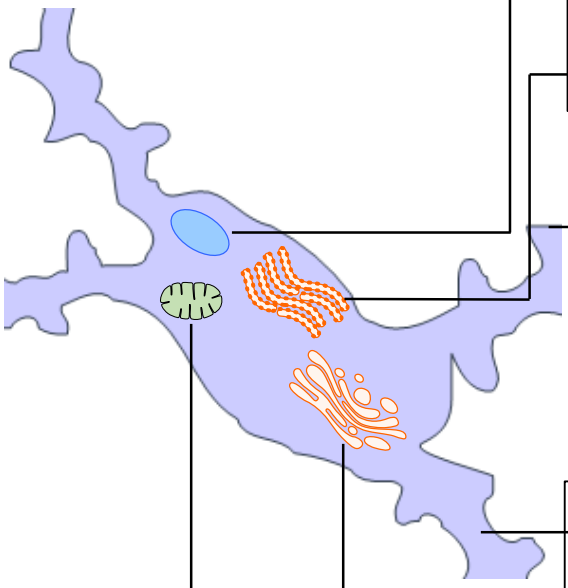

Transcription
Bcas2, Churc1, Cic, Cops5, Creb3, Cux1, Ddx1, Drap1, Ebna1bp2, Eprs, Exosc9, Fcf1, Hmgn3, Ipo5, Mbd2, Mina, Mxd4, Naca, Npat, Phf11d, Prpf6, Ptbp1, Pus3, Rbm42, Rpp38, Rtcb, Scand1, Scnm1, Setd3, Snf8, Snord38a, Snrpd3, Snrpe, Snrpf, Syncrip, Synj2, Taf10, Taf5l, Tatdn2, Tceb2, Trim30a, Utp11l, Utp14a, Yaf2, Znhit1, Znrd1

DNA Binding/Repair
1200014J11Rik, Apitd1, Dek, Dmrtc1c, Dnmt3a, Dscc1, Eya4, Fam50a, Mir29a, Mirn692-2b, Nono, Rps27, Parp14, Pgap1, Rlf, Sap30, Trip12, Uba52, Utp3, Xrn2, Zbp1, Zcchc17

General Metabolism
1700021F05Rik, 1810037I17Rik, 2010107E04Rik, Akr1a4, Alas1, Atl2, Azin1, Bhlhb9, Casd1, Dpy19l4, Enpp1, Erbb2ip, Evi2a, Extl3, Fam165b, Fam174a, Fundc2, Gm10063, Impad1, Lsmd1, Ly6e, Mcee, Mrpl39, Mrpl52, Mrps33, Mrps9, Naa20, Naa50, Nd1, Ndufa8, Ndufb2, Ndufb5, Oxct1, Pde4dip, Pgam1, Ppm1m, Smpdl3a, Surf4, Tor3a, Vkorc1, Wbp5,

Translation
Eef1b2, Eif1a, Eif2s2, Eif3e, Eif3h, Eif3k, Eif3l, Eif4b, Etf1, Fau, Gm6251, Lsm2, Mrpl22, Mrpl34, Mrpl36, Mrrf, Naf1, Oas1g, Oasl2, Rpl10a, Rpl11, Rpl12, Rpl13, Rpl13a, Rpl14, Rpl18a, Rpl19, Rpl21, Rpl22, Rpl22l1, Rpl26, Rpl27, Rpl27a, Rpl28, Rpl3, Rpl31, Rpl32, Rpl35, Rpl35a, Rpl36, Rpl36a, Rpl36al, Rpl37, Rpl37a, Rpl38, Rpl39, Rpl39l, Rpl4, Rpl41, Rpl5, Rpl6, Rpl7, Rpl8, Rplp0, Rps10, Rps11, Rps12, Rps14, Rps15a, Rps15a-ps6, Rps16, Rps17, Rps18, Rps19, Rps2, Rps20, Rps21, Rps23, Rps25, Rps26, , Rps27a, Rps27l, Rps29, Rps3, Rps3a, Rps4x, Rps5, Rps6, Rps7, Rps8, Sart3, Sec61b, Sec63,

Lipid Processing (membrane)
Abca1, Acbd6, Acot10 , Anxa3, Aplp2, Apob, Apobec1, Apoc1, Apoe, Ch25h, Chchd3, Fam167b, Gde1, Gltp, Lrpap1, Msr1, Osbpl8, Pcyt1a, Peci, Pld3, Plin2, Ppap2a, Ptgfrn, Ptgs2, Ptplad2, Sgpl1, Srd5a3, Ttc1,

Ion Binding/Transport (membrane)
4931406C07Rik, Aif1, Anxa4 Anxa5, Asph, Atp13a5, Atp1a3, Atp2b1, Calu, Ccdc90a, Cmc1, Cox17, Dnlz, Fus, Fxyd5, Gca, Gnb2l1, Kctd2, Ndufv1, Nme1, Nucb1, Nucb2, rp9, Sdf4, Slc11a2, Ssr4, Tpd52, Vwce, Zfp704, Zfp868

Protein Processing (Inc. Proteasome)
Cndp2, Cpd, Cuedc2, Cul4b, Derl1, Dnajb14, Erlec1, Fbxw4, Isg15, Mmp12, Nedd8, Pfdn1, Pfdn5, Psma7, Psmb1, Psmb2, Psmb3, Psmb4, Psmb6, Psmd8, Psme1, Ptpra, Rbx1, Shfm1, Spcs1, St14, St8sia6, Tceb1, Tcp1, Ubl5,

Protein Transport (Inc. Vesicular)
Ap3s1, Arl6ip5, Bst2, Cct2, Chmp1b, Chmp7, Exoc2, Golim4, Golph3, Gosr2, Mfsd1, Mmgt2, Mtmr2, Myl6, Nipsnap3b, Nup98, Plekha3, Rab1b, Rap2a, Rap2b, Rasgef1b, Rer1, Rtp4, Slc23a2, Slc38a6, Slc6a6, Slc7a11, Snap29, Snx17, Snx24, Snx3, Srp14, Srp72, Tbc1d22a, Tmed3, Vps28, Vps29, Vti1b,

Carbohydrate Metabolism
Chst1, Chst11, Chst2, Galnt6, Galnt7, Gcnt2, Gfpt1, Gmds, Gnpda2, Gnptab, Gyg, Pfkfb3, Pfkl, Pgk1, Pigl, Pigu, Prkar1a, Tpi1,

Energy Production
2700094K13Rik, Acadl, Adap1, Atp5e, Atp5h, Atp5k, Atp5l, Cox5b, Cox6a1, Cox6a2, Cox6b1, Cox7a1, Cox8a, Cybb, Cycs, Cyp4v3, Fdx1, Glrx5, Gm10136, Grpel1, Higd1a, Higd2a, Hsd17b11, Idh1, Ldha, Ldhb, Ndufa1, Ndufa2, Ndufa3, Ndufa4, Ndufa6, Ndufb11, Ndufc2, Ndufv3, Prdx4, Romo1, Slc25a4, Surf1, Tmx3, Tomm7, Txndc5, Uqcr10, Uqcrb, Uqcrh, Usmg5, Vat1, Xdh

Figure 9